The dependence of $\Psi(\nu, k)$ on the magnetic field is shown in Fig. 2 for two different values of η^2. The resistive plasma loading of a Stix coil has been estimated for a plasma cylinder in a uniform magnetic field with ω equal to or very close to Ω_i. In a toroidal configuration the main modification, if natural modes are not considered, would be in the imaginary part of $K_\perp{}^2$, which varies as $\exp(-\zeta_1{}^2)$. Since the power absorption is proportional to $\mathrm{Im}[K_\perp{}^2]$, at least for $\mathrm{Im}[K_\perp{}^2] \ll \mathrm{Re}[K_\perp{}^2]$, it reduces rapidly to zero as $|\zeta_1|$ increases; see Fig. 2. In this case electron Landau damping, a second-order effect for $|\zeta_1| \lesssim 1$, can no longer be ignored.

In a toroidal magnetic field we have $\zeta_1 = (R - R_0)\zeta_0/R$, R_0 being the radius at which $\omega = \Omega_i$, so that only a fraction $\alpha \approx R_0/\zeta_0 P$ of the total plasma volume will be heated and the resistive impedance of the coil decreases accordingly:

$$R_p{}^{\mathrm{eff}} = \alpha R_p .$$

For $|\zeta_1| \lesssim 1$, electron Landau damping is of the order $\epsilon = T_e/4T_i\zeta_0$ with respect to ion cyclotron damping; however, it is almost uniform over the whole plasma volume, so that the effective contribution of electrons to the total power absorption will be approximately $\beta \approx T_e p/4T_i R_0$ with respect to one of the ions.

It is evident that the method presented here is more efficient in toroidal configurations with very low aspect ratio such as stellarators. However, for Tokamak parameters[4] as well, the greater part of the rf power will be absorbed by the ions and, although only a small fraction of the plasma volume will be heated, the method proposed here still remains attractive; it is, for example, a few orders of magnitude more efficient than transit-time magnetic pumping.[5]

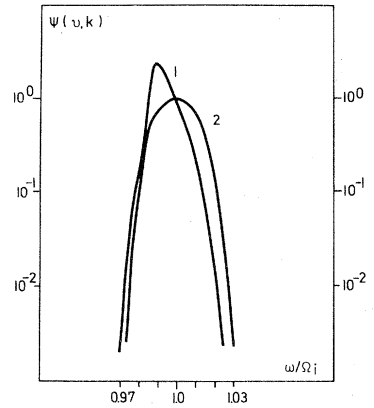

FIG. 2. $\Psi(\nu, k)$, normalized to 1 at $\omega = \Omega_i$, vs ω/Ω_i for $\zeta_0 = 10^2$, $k_\parallel p = 1$, and (curve 1) $\eta^2 = 10^{-2}$ or (curve 2) $\eta^2 = 20$.

[1]T. H. Stix, *The Theory of Plasma Waves* (McGraw-Hill, New York, 1962).
[2]M. A. Rothman, R. M. Sinclair, I. G. Brown, and S. C. Hosea, Phys. Fluids 12, 2211 (1969).
[3]M. F. Uman and W. M. Hooke, Phys. Fluids 12, 1072 (1969).
[4]M. J. Forrest, N. J. Peacock, D. C. Robinson, V. V. Sannikov, and P. D. Willcock, Culham Report No. CLM-R 107, 1970 (unpublished).
[5]J. M. Dawson and M. F. Uman, Nucl. Fusion 5, 242 (1965).

High–Mach-Number Turbulent Magnetosonic Shocks

K. Papadopoulos, C. E. Wagner, and I. Haber
Naval Research Laboratory, Washington, D. C. 20390
(Received 9 August 1971)

High–Mach-number turbulent magnetosonic shocks caused by driving a purely reflecting piston into a plasma have been simulated using an electromagnetic particle code. A physical analysis of the results is presented together with scaling arguments and comparisons with experimental data.

Fluid theories incorporating a phenomenological anomalous resistance seem to account for the basic observations on low–Mach-number ($M_A \lesssim 3$) shocks.[1,2,3] However, the use of similar techniques has not been successful for the case of high-M_A shocks.[1,2] It appears that computer simulation offers today the most promising technique for understanding such structures.[2] In this Letter we present the first two-species self-consistent particle simulation of the formation and evolution of a high-M_A "viscous" magnetosonic shock. Previous particle studies were performed for purely electrostatic ($B_0 = 0$)[4] or laminar[5] shocks. We restrict our simulation results to situations of zero resistivity. This allows for clear indentification of the turbulent ion-ion in-

teractions without the complexities added by electron-ion–induced turbulence. For the case with zero resistivity under consideration the critical M_A for fluid breaking is[1] $M_c \sim 1$. The effects of finite anomalous resistivity are incorporated in the physical discussion presented at the end of the Letter.

We start with the simulation results since they provide the means of positively identifying the physical mechanisms operating in the shock front. A qualitative discussion of the physics involved, theoretical conclusions, and a comparison with experiments follow.

Numerical experiments.—The numerical experiments were performed with a one-dimensional particle code.[6] The electrons were followed in their self-consistent *electromagnetic* orbits while the ions were followed in their electrostatic orbits only. The effect of the magnetic field was not included in the ion dynamics because we are interested in length scales shorter than an ion Larmor radius. The shocks were created by moving a perfectly reflecting piston into the plasma with velocity corresponding to piston Mach number $M_p = V_p/V_A = 1.5$–2.5. Since the particles are reflected with velocity $2V_p$, we expect shock formation with[7] $1.5 \leq M_A \leq 5$. In the cases discussed here, each electron and ion species is represented by $(2.5$–$5)\times 10^4$ simulation particles which move on a grid of 1024 cells. The electron-ion mass ratio was $m/M = 10^{-2}$, the length $c/\omega_e = 7$ cells, and the time step $\Delta t = 0.2\omega_e^{-1}$.

Since the simulation is one-dimensional, only instabilities with wave vectors $\vec{k}$ in the x direction are allowed. Thus waves causing anomalous resistance which derive from the diamagnetic electron current and propagate in the y direction will not be present. The possibility of strong electron-electron or electron-ion interactions[8] was also eliminated by giving to the electrons thermal velocity $V_e \sim V_p$. Figure 1 shows the results of various diagnostics for two typical runs.

Shock formation and evolution.—The reflection of particles from the piston creates two counterstreaming ion beams within the region of compressed magnetic field without any appreciable increase in their thermal energy [Figs. 1(a) and 1(b)]. This is a transient state during which the reflected electrons interact laminarly with the magnetic field and the ambient electrons to produce the observed field compression. This counterstreaming situation, as was demonstrated recently,[9] is unstable to electrostatic ion waves, and results in coupling the ion streams within distances of the order c/ω_e. The role of this instability in experiments has been discussed by

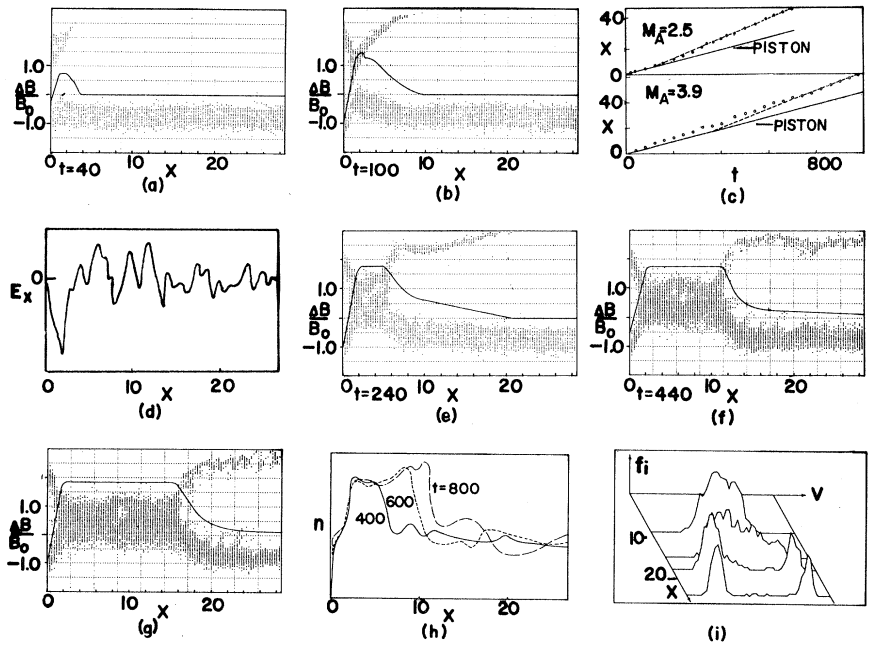

FIG. 1. (a), (b) Ion phase space and magnetic field profile before shock formation ($M_A = 2.5$). (c) Piston versus shock separation as a function of time ($M_A = 2.5$ and 3.9). (d) Spatial evolution of ion turbulence ($M_A = 3.9$). (e)–(g) Ion phase space and magnetic field profile during steady state ($M_A = 2.5$). (h) Time evolution of the density profile ($M_A = 3.9$). (i) Ion distribution function inside the transition length as a function of space ($t = 900\omega_e^{-1}$, $M_A = 3.9$).

Davis *et al.*[10] and by Dean *et al.*[10] The piston subsequently is transformed into an essentially "snowplowing" one. Ion pressure gradients resulting from the ion thermalization cause the leading edge of the disturbance to travel at a velocity higher than that of the center of mass, while the trailing edge moves slower. This leads to the classic shock-wave–piston separation [Fig. 1(c)]. Ion waves generated in the unstable region near the piston move ahead and constitute a momentum-carrying mechanism in addition to the ion pressure gradients. These waves are shown in Fig. 1(d). The time for the formation of a steady-state structure appears to depend critically on the M_A and is presently under study. Figures 1(e)–1(g) show the formation of the steady-state structure. Figure 1(h) shows the evolution of the density profile at various times. The magnetic profile (not shown here) is similar, confirming the fact that for "viscous" shocks $B(x) \propto n(x)$.

The maintenance of a self-consistently supported steady state [Fig. 1(i)] is consistent with speculations presented by Tidman for pure electrostatic shocks.[2,11] The hot ion gas drifts slowly downstream while trying to expand upstream. In expanding upstream it encounters the incoming cold ion stream and produces the unstable distribution in the front edge of the hot layer. This can be seen from Fig. 1(i) and also from the ion phase-space figures [Fig. 1(e)–1(g)]. Incoming ions continuously plow into the hot ion gas and regenerate it, maintaining the turbulent transition.

Another feature of the results shown is the "footlike" structure in the magnetic front. The potentials measured across the front are not large enough to reflect ions ($e\varphi/\frac{1}{2}Mu^2 \ll 1$), and are consistent with the condition that the magnetic field is frozen into the plasma. One can see, however [Figs. 1(a), 1(b), 1(e), 1(f)], that this foot is not part of a steady-state formation connected with ion reflection from the front, but it is due to ion acceleration in the piston region, mainly before the ion turbulence had time to develop. These ion streams are subsequently stable since they exist in regions of low field compression and they stream freely while they disperse in space because of their thermal spread. Besides this initial foot formation a few ions will continuously leave the tail end of the downstream distributions. However, the simulations show that these are not enough to provide an observable effect at high M_A.

Finally we note that the Hugoniot conditions were very closely satisfied for the observed density and field jumps, with the pressure controlled by ion heating.

Conclusions.—The following qualitative conclusions can be reached from the previous picture: (i) The counterstreaming *electrostatic* ion instability across the magnetic field has been clearly identified as the source of ion dissipation both in the shock and the piston regions. (ii) The mixing of the upstream and downstream states allows a continuous regeneration of ion distributions capable of maintaining a turbulent transition. (iii) The steady-state high-M_A shock structure does not depend on direct interaction of the magnetic field with the ions. (iv) The potentials in the shock front are not large enough to reflect ions. Therefore foot structures in shocks with high downstream ion pressure should be due to either reflection from the piston before the steady-state shock was formed, or acceleration in the region behind the shock front. (v) The formation of a shock from a collisionless piston depends critically on the existence of ion dissipation in the piston region in agreement with various θ-pinch experiments. (vi) The lengths that will control the collisionless front are the distance x_0 (Fig. 2) which brings us from the stable region to the unstable one, and the ion thermalization length L_H. Since $B(x) \propto n(x)$, the length x_0 will be given by

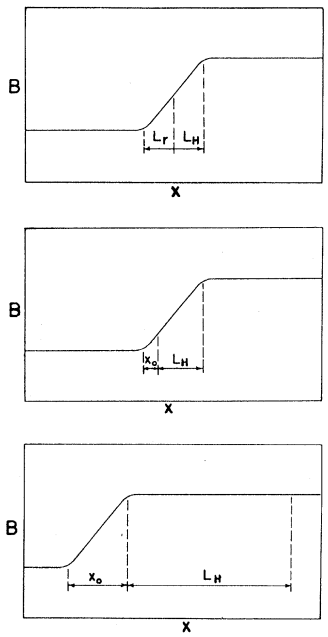

FIG. 2. Typical profile of the three classes of magnetosonic shocks.

the solution of the equation[9,12]

$$\left[1-\frac{B(x_0)}{B_0\eta}\right]\left[\frac{B(x_0)}{B_0}\right]^{1/2}=\frac{2.5}{M_A}, \quad (1)$$

where η is the upstream-to-downstream compression ratio and $B(x)$ the magnetic field profile. Both can be determined experimentally. The length L_H can be found from the nonlinear theory of the ion-ion instability and is given by[9]

$$L_H=3(M/m)^{1/2}u_1/\Omega_{el}. \quad (2)$$

Comparison with experiments.—In order to compare the above model with the experiments, we separate the magnetosonic shocks into three broad classes according to their M_A. For $3\lesssim M_A\lesssim 4.5$, the resistive electron heating is of the order of the viscous ion heating ($\Delta T_e/\Delta T_i\sim 1$). We would therefore expect a transition length scale

$$L\sim L_r+L_H, \quad (3)$$

where L_r is the resistive length [Fig. 2(a)]. Assuming a profile

$$B(x)=B_0[e^{-x/L}+\eta(1-e^{-x/L})], \quad (4)$$

and using Eq. (1), we find that for

$$4.5\leq M_A<7.5\sqrt{3}\,[\eta/(\eta-1)](1+2\eta)^{-1/2}, \quad (5)$$

the length x_0 will basically be at the front tip of the magnetic transition [Fig. 2(b)] and the shock profile will be controlled by the ion heating length

$$L\sim L_H. \quad (6)$$

Finally for

$$M_A>7.5\sqrt{3}\,[\eta/(\eta-1)](1+2\eta)^{-1/2} \quad (7)$$

the magnetic transition takes place first with a length of order x_0 [Fig. 2(c)] while the ion heating occurs far downstream after the magnetic transition with $L_H\gg x_0$. In this case there are two clearly separate length scales. The length scale x_0 controls $B(x)\propto n(x)\propto u(x)$ while the ion heating takes place in an isomagnetic fashion [$B(x)\propto n(x)\sim$const, $T_i(x)$ increasing] far downstream with scale L_H.

In Table I we present a comparison of the above qualitative theory with various experiments. The first three experiments[13] belong to the first class. By subtracting L_H from the experimentally measured length, one can deduce the resistive length L_r. As shown in Table I, for all three experiments $L_r\sim 35$ cm $\sim 11c/\omega_e$, which is in agreement with the accepted resistive length. The subsequent eight experiments[14-16] belong to the second class [Eq. (5) is satisfied for all cases]. Typical of the third class is the bow shock. Satellite measurements have resolved $x_0\sim 1$ km and $L_H\sim 40$–80 km. A detailed theory modified for the fact that $\beta_e\sim 1$ has already been presented elsewhere,[17] and is in good agreement with the present model. Experimental measurements of this class of shocks are not very conclusive since the separation of piston and shock is small within the experimental radius.

TABLE I. Comparison of experimental data with theory.

Ref.	M_A	L_{exp} (cm)	L_H (cm)	$L_r=L_{exp}-L_H$ (cm)
13	3.6	0.50	0.24	0.36
13	3.8	0.63	0.29	0.34
13	4.25	0.68	0.32	0.36
15	4.5	0.65	0.55	•••
14	4.7	2.0	1.7	•••
14	5.6	2.4	2.7	•••
14	6.3	3.1	2.9	•••
1	6.3	0.30	0.39	•••
14	8.3	2.3	2.7	•••
15	8.7	1.7	1.8	•••
16	7	0.8	1.2	•••

In a future publication we will present a quantitative analytic theory of the shock structures, the time of their formation from a piston, and a critique of the conditions for which an anomalous viscosity can be used within the framework of a two-fluid or multifluid theory.

We wish to acknowledge several useful discussions with Dr. D. Book, Dr. J. P. Boris, Dr. T. Coffey, Dr. G. Goldenbaum, Dr. E. Hintz, Dr. R. Shanny, and Dr. D. Tidman.

[1]J. W. M. Paul, in *Physics of Hot Plasmas*, edited by B. J. Rye and J. C. Taylor (Plenum, New York, 1970), Chap. 8.

[2]D. A. Tidman and N. A. Krall, *Shock Waves in Collisionless Plasmas* (Wiley, New York, 1971).

[3]N. A. Krall and D. L. Book, Phys. Rev. Lett. 23, 574 (1969).

[4]S. A. Colgate and C. W. Hartman, Phys. Fluids 10, 1288 (1967); see also J. Dawson, K. Papadopoulos, and R. Shanny, Phys. Fluids 13, 1650 (1970).

[5]D. W. Forslund and C. Shonk, Phys. Rev. Lett. 25, 1699 (1970).

[6]I. Haber, C. Wagner, J. Boris, and J. M. Dawson, in Proceedings of the Fourth Conference on Numerical Simulation of Plasmas, Washington, D. C., 1970, edited by R. Shanny and J. Boris (U. S. GPO, Washington, D. C., to be published).

[7]Because of computer limitations we were restricted to this range of M_A. However, the philosophy of the paper is to demonstrate the physical mechanisms operating in cases where electron heating is small, which is the case for laboratory experiments with $M_A > 4$.

[8]R. C. Davidson, N. A. Krall, K. Papadopoulos, and R. Shanny, Phys. Rev. Lett. 24, 579 (1970).

[9]K. Papadopoulos, R. C. Davidson, J. M. Dawson, I. Haber, D. A. Hammer, N. A. Krall, and R. Shanny, Phys. Fluids 13, 849 (1971). See also C. Wagner, K. Papadopoulos, and I. Haber, Phys. Lett. 35A, 440 (1971).

[10]W. D. Davis, A. W. DeSilva, W. F. Dove, H. R. Griem, N. A. Krall, and P. C. Liewer, in Proceedings of the Fourth Conference on Plasma Physics and Controlled Nuclear Fusion Research, Madison, Wisconsin, 1971 (to be published); S. O. Dean, E. A. McLean, J. A. Stamper, and H. R. Griem, Phys. Rev. Lett. 27, 487 (1971).

[11]D. A. Tidman, Phys. Fluids 10, 547 (1967).

[12]Equation (1) derives from Eq. (28) of Ref. 9; the factor 2 has been replaced by 2.5 which is the proper factor for the two-dimensional theory of the instability.

[13]S. E. Segrè and M. Martone, Plasma Phys. 13, 113 (1971).

[14]A. W. DeSilva, W. F. Dove, G. C. Goldenbaum, and I. J. Spalding, Phys. Fluids 14, 42 (1971).

[15]P. Bogen, K. J. Dietz, K. H. Dippel, E. Hintz, K. Höthker, and G. Zeyer, in Proceedings of the Fourth Conference on Plasma Physics and Controlled Nuclear Fusion Research, Madison, Wisconsin, 1971 (to be published).

[16]E. Hintz, in *Plasma Physics and Controlled Nuclear Fusion Research* (International Atomic Energy Agency, Vienna, Austria, 1969), Vol. 1, p. 69.

[17]K. Papadopoulos, J. Geophys. Res. 76, 3806 (1971).

Core Structure of a Quantized Vortex*

Alexander L. Fetter†
Institute of Theoretical Physics, Department of Physics, Stanford University, Stanford, California 94305
(Received 7 September 1971)

The core of a singly quantized vortex is shown to consist of both condensed and noncondensed particles. Model calculations with an imperfect Bose gas suggest a plausible core structure in liquid helium.

Recent experiments have demonstrated that the mobility of ions trapped on vortex lines in rotating superfluid helium is markedly less than that of untrapped ions.[1,2] These data imply the existence of additional drag forces near the vortex axis, but the detailed interpretation depends on particular models of the vortex core and its interaction with the ion.[2-4] To clarify this situation, we here study the core structure of a quantized vortex line. Although the conclusions are derived from an imperfect Bose gas, the essential physical features are model independent and should apply equally well to superfluid helium.

Consider N bosons of mass m in a volume V interacting through a short-range potential $v(\vec{r}-\vec{r}') \approx g\delta(\vec{r}-\vec{r}')$. The simplest description is the Hartree approximation, where the free-particle Schrödinger equation is augmented by a potential energy $gN|\psi|^2$ proportional to the particle density. Here ψ is a normalized single-particle wave function, and the N-body ground state is obtained by putting all the particles into the lowest single-particle state ψ_0. For a uniform system with periodic boundary conditions, we clearly have $\psi_0 = V^{-1/2}$; for a singly quantized vortex, the appropriate choice is $\psi_0 = V^{-1/2} e^{i\theta} f(r)$, representing a state with unit angular momentum about the z axis. The real radial function f satisfies the nonlinear Gross-Pitaevskii equation,[5,6] with the approximate behavior

$$f(r) \propto r/\xi, \quad r \to 0, \qquad f(r) \sim 1 - \xi^2/2r^2, \quad r \to \infty, \tag{1}$$

where ξ is a characteristic length defined by $\xi = \hbar(V/2mNg)^{1/2}$. The corresponding N-body wave function in configuration space is given by

$$\Psi_H(\vec{r}_1, \cdots, \vec{r}_N) = \prod_j [V^{-1/2} e^{i\theta} f(r_j)], \tag{2}$$

where the product runs over all the particles in the system. Equation (2) is an eigenstate of L_z with eigenvalue $N\hbar$, and it readily yields the physical properties of the N-body system. For example, the density $n(r) = NV^{-1}|f(r)|^2$ vanishes quadratically for small r and approaches the bulk value $n \equiv N/V$ at infinity. The circulating current is given by $j(r) = n(r)\hbar/mr$, which rises linearly for $r \lesssim \xi$, reaching a maximum of order $n\hbar/m\xi$, and falls like $n\hbar/mr$ for $r \to \infty$. By definition, the ratio of these two expectation values is the circulating velocity field $v(r) = \hbar/mr$, denoting a singly quantized vortex with circula-